JOINT EUROPEAN TORUS JET

JET–P(93)29

J.P. Christiansen, J.G. Cordey, A. Taroni.

The Testing of Transport Models against Data

The Testing of Transport Models against Data

J.P. Christiansen, J.G. Cordey, A. Taroni.

JET-Joint Undertaking, Culham Science Centre, OX14 3DB, Abingdon, UK

Preprint of a paper to be submitted for publication in
Nuclear Fusion
April 1993

ABSTRACT

A large number of theoretical, heuristic and empirical models for transport in a Tokamak have been developed. Many models have been claimed to adequately describe subsets of the wealth of data accumulated from several Tokamak experiments. Yet no single transport model has emerged as an obvious candidate that will give an accurate extrapolation from today's large Tokamaks to a reactor. It is shown how this situation can arise from three features associated with the testing of models against experimental data: i) measurement errors, ii) collinearities in the data and iii) confinement degradation with power. These features, when combined, permit the claims that a variety of transport models based on different physics can fit the data. It is proposed that transport models should be tested against data from experiments in which only one dimensionless plasma parameter is being varied at a time. Such experiments include the scans carried out on DIIID, TFTR and JET of the parameters ρ_* (normalised Larmor radius), ν_* (collisionality) and β. It is also shown that the testing of transport models must include data from two or more Tokamaks of different size in order to separate model predictions by more than the experimental measurement error level.

1. INTRODUCTION

The first generation of Tokamaks, T3, ST, ATC, ORMAK, CLEO, produced diagnostic data mainly in the form of global measures such as the stored energy, loop voltage etc. The testing of transport models against experimental Tokamak data, which is the subject of this paper, was hence rather limited and inconclusive, as described in the reviews of computational studies [1] and of computer models [2]. The early models [3] were based on classical transport theory but needed additional non-classical physics in order to match data from the second generation of Tokamaks like TFR, T-10, PLT, DITE, JFT2, ISXB, ASDEX and PDX. The article by Hugill [4] reviews some of the theoretical-computational efforts that were needed to explain the plasma energy loss rate which was observed to be non-classical; specific models could be tested against data from e.g. PLT-PDX [5], ASDEX [6] etc. The third generation of large Tokamaks, JET, TFTR, DIIID, JT60, Tore-Supra and JT60U can all produce the essential ingredients required for meaningful tests of plasma transport models: time and spatially

resolved profiles of density, temperatures, radiation, Z_{eff}, x-ray emission, safety factor. A concurrent development of many transport models has taken place: empirical models explaining the scaling of global confinement [7-9], heuristic models featuring a mixture of theory and experimental observations [10-11] and purely theoretical predictions. The latter include too many references to quote and the reader is referred to a recent article "Survey of theories of anomalous transport" by Connor and Wilson [12].

Given the wealth of Tokamak data, why is it that no single transport model has emerged as an obvious candidate for extrapolations towards a reactor regime from the available data? This paper will address this question by examining in this detail what tests of transport models against local and global data involve. The aim of the study is to establish what constitutes a meaningful and successful test of a model such that an accurate extrapolation to a reactor regime can confidently be made.

In section 2 we put forward a description of the thermal flux and diffusivity in a Tokamak starting from the scale invariance approach to confinement scaling of Kadomtsev [13] and Connor-Taylor [14]. The dimensionally correct forms for heat flux q and diffusivity χ include an unknown function of dimensionless parameters. This prescription is used in section 3 to establish the link between global and local confinement using a one fluid treatment. The properties of Tokamak data, in particular JET data, are highlighted in section 4 with an emphasis on the data collinearities which affect transport model testing. The link between local and global confinement (section 3) is applied in section 5 to analyse the testing of transport models against global data; in section 6 we perform a similar analysis of tests against local JET profile data. The results from both sections demonstrate how it becomes possible for different physics models to reproduce the data values when allowance is made for experimental measurement errors. It is the experimental errors and collinearities in the data being tested combined with confinement degradation with power that make the tests insensitive to the details of a given transport model. An undesirable implication of this result arises when extrapolations towards a reactor are made with models which can reproduce present global or local data; we illustrate this point in section 7 using the ITER L-mode database.

In the concluding section 8 we therefore put forward arguments for testing transport models against data in which only one dimensionless parameter is

being varied. Such data can be obtained from the Tokamak discharge scans of ρ_* (normalised Larmor radius), ν_* (normalised collisionality) and β carried out on DIII D [15], TFTR [16] and JET [17]. We emphasise that a test of a transport model must involve data from more than one Tokamak and to facilitate such test we propose the assembly of a multi-machine local transport data base. In this paper we use SI units with temperatures in eV.

2. TRANSPORT THEORY

The power flow per unit area across a surface x, where $0 \le x \le 1$ denotes a non-dimensional flux surface label of a Tokamak equilibrium configuration, is given by the expression

$$q = - en_e \chi_e \nabla T_e - en_i \chi_i \nabla T_i + q_{flow} \tag{1}$$

in which the temperature gradients are averaged over a flux surface and the thermal diffusivities χ_e, χ_i are local functions. The flow given by (1) includes a thermal and a non-diffusive part. In the present study we shall omit the non-diffusive component q_{flow} associated with convection or a heat pinch; for many JET plasmas $q_{flow} << q_e + q_i = q$ as demonstrated by recent on-off axis heating experiments on JET [18]. We choose a one fluid reactor relevant regime with temperatures $T_e = T_i = T$ and densities n_e close to n_i (D,T, ^{4}He). The total thermal flux therefore becomes

$$q = q_e + q_i = - en \chi \nabla T \tag{2}$$

in which the effective thermal diffusivity χ is some function of the local plasma variables. The most basic plasma model is that described by the collisionless Vlasov equation in the electrostatic limit. For this model one obtains [14]

$$\chi = \chi_B \, F\left(\rho_*, p_{geom}\right), \quad \chi_B = T/B, \quad \rho_* = \rho/a \tag{3}$$

The diffusivity χ_B is Bohm diffusion coefficient and ρ_* is the Larmor radius ρ normalised by minor radius; both χ_B and ρ will be defined in terms of $B = B_p$ the poloidal field (see Appendix A), p_{geom} denotes any dimensionless parameter involving only the plasma geometry, e.g. inverse aspect ratio $\varepsilon = a/R$, elongation E etc. The unspecified function F may be determined from the physics of the transport model adopted: for example if FLR effects are omitted ($\rho_* \to 0$), as in the

two dimensional guiding centre model [19], then F reduces to F = F (a/L) where L is a length scale in the direction of B. In order to allow for more complex plasma physics, e.g. collisions, non-electrostatic effects, the simple model (3) must be replaced by the general expression.

$$c = \chi_B F\left(\rho_*, \nu_*, \beta, \varepsilon, q_\psi, p_1, p_2, \ldots\right) \tag{4}$$

A subset of the possible arguments of F are defined in Appendix A and denoted by p_1, p_2... etc. We have excluded dimensionless parameters which are based on atomic and radiation physics, e.g. parameters which depend on the Debye length λ_D, plasma frequency ω_p, ionisation energy E_z etc. The reason for this omission is that global confinement data from several Tokamaks of different sizes has been demonstrated [9] to satisfy the constraint imposed by the High-β Fokker-Planck model. This constraint [13] requires that the global confinement time τ_E does not depend on the very short scale length $L \sim \lambda_D$.

From the general expression (4) we can recover forms of χ which have a different physical origin (see [12, 20]): e.g. resistive MHD transport model characterised by a resistivity η can be transformed as

$$\chi_{MHD} = \frac{\eta}{\mu o} F_1(\ldots) = \chi_B \rho_* \nu_* \beta^{-1} F_2(\ldots)$$

i.e. transformed to the form (4). The local dimensionless parameters in Eq. (4) feature in their definitions (see Appendix A) minor radius a which is a non-local variable; in principle a can be replaced by a local measure such as $L_n = n/\nabla n$. The use of minor radius a is customary and it connects the definitions of the local parameters with the corresponding global averages defined in Appendix B.

3. THE LINK BETWEEN τ_E AND χ

In order to examine what is involved in a test of a local transport model against global data, we establish in this section some expressions that will be used later. The global confinement time τ_E and integrated power deposition profile are given by

$$\tau_E = \frac{1}{P}\int_0^1 3enT\ V'\ dx \quad , \quad P(x) = \frac{1}{a}\ V'\ q(x) \tag{5}$$

where P = P(x = 1) is the total power input. We use the partial integration method of Callen et al. [21] and note that $\nabla T = dT/dx\ |\nabla x|^2$, via the geometry factor $|\nabla x|^2$ is averaged over a surface; (for an equilibrium of shifted elliptic surfaces with ellipticity E(x) one gets $|\nabla x|^2 = 2E^2/(a^2(E^2 + 1))$. The result from (5) becomes

$$\tau_E = \frac{1}{P}\ 3e\ N_1T_1 + \frac{1}{P}\int_0^1 \frac{N(x)\ P(x)\ dx}{n(x)\ V'\ |\nabla x|^2\ \chi} \tag{6}$$

where $N(x) = \int_0^x n\ V'\ dx'$ and subscript 1 implies x = 1 for brevity. From the definitions in Appendix B of the global averages of those dimensionless parameters given in Appendix A we can recast the above expression in terms of the profile shapes

$$n(x) = \langle n \rangle g_n(x)\ , \quad N(x) = \langle n \rangle V\ g_N(x)\ , \quad T(x) = \langle T \rangle g_T(x) \tag{7}$$

$$P(x) = P\ g_P(x)\ , \quad B(x) = \frac{\mu_o I_\varphi}{2\pi a}\ g_B(x)$$

The angular brackets denote appropriate volume averages (Appendix B). The relation between τ_E and χ can now be expressed in a form which directly reflects Eq. (4)

$$\tau_E = \tau_1 + \tau_B\ G\ , \quad G = \int_0^1 \frac{g\ (x)}{F(p_j)}\ dx \quad , \quad g(x) = a^2|\nabla x|^2\ \frac{g_N\ g_P\ g_B}{g_n\ g_T} \tag{8}$$

We have set $\tau_1 = 3eN_1T_1/P$ and for L-mode plasmas $\tau_1 << \tau_E$, e.g. for JET $\tau_1 \sim 10^{-3}$ - $10^{-2}\ \tau_E$ typically. From global fits to confinement data [7-9] we notice that the dimensionless parameter G is $O(10^3)$; The geometry factor is O(1) while the profile shape ranges from typically 0 to 5; we thus expect $F \sim O(10^{-3})$. Local transport models can be expressed as [12, 20]

$$F = \rho_*^{x_\rho}\ \nu_*^{x_\nu}\ \beta^{x_\beta}\ q_\psi^{x_q}\ f(p_j) \tag{9}$$

in which $f(p_j)$ mimics any residual dependence of F upon parameters such as ε_n, ε_T, S, A, etc. We substitute the relations in Appendix B between e.g. ρ_* and $<\rho_*>$, insert (9) into (8) and solve Eq. (8) for τ_E in the limit $\tau_1/\tau_E \to 0$. The result is

$$\tau_E = \left(\tilde{\tau}_B \tilde{G}\right)^{1/(x_\tau+2)} \quad , \quad x_\tau = \tfrac{1}{2}x_\rho - 2x_\nu + x_\beta \tag{10a}$$

The tilde symbols are intended to indicate that τ_E has been removed from the definition of τ_B as well as from those for $<\rho_*>$, $<\nu_*>$, $<\beta>$ contained in G via F given by (9). The relation (10a) which is explicit in τ_E can also be written in the power law form

$$\tau_E = C\, a^{z_a} <n>^{z_n} I_\phi^{z_I} P^{z_\rho} \varepsilon^{z_\varepsilon} \kappa^{z_\kappa} A^{z_A} \tilde{G}^{1/(x_\tau+2)} \tag{10b}$$

where the exponents z_a, z_n etc. depend on x_ρ, x_ν, x_β as shown in [9]. Empirical scaling laws [7-9] are usually represented as (10b) but without the profile term $\tilde{G}$. We notice in the global scaling expression (10a) that the profile effects arising from F given by (9) are suppressed via "the power degradation" index $x_\tau + 2$. In Appendix C we list twelve theoretical, heuristic and empirical scalings and give the resulting value for $x_\tau + 2$. Theoretical scalings for F usually take the form (9) but it has also been demonstrated [22] that 20 empirical scaling laws for τ_E originate from Eq. (9). Together with the theoretical models they fall mainly in two categories:

$$\begin{aligned} &\text{I. Empirical, Bohm like} && : \ x_\rho = 0, \ x_\nu \gtrsim 0, \ x_\beta > 0 \\ &\text{II. Theoretical, heuristic, gyroBohm like} && : \ x_\rho = 1, \ x_\nu \lesssim 0, \ x_\beta < 0 \end{aligned} \tag{11}$$

4. PROPERTIES OF THE DATA

Global confinement data from a range of second and third generation Tokamaks is available in the ITER L-mode and H-mode databases. When such data is represented in terms of the global averages $<\rho_*>$, $<\nu_*>$, $<\beta>$ and q_ψ inner relations or data collinearities are present; these dimensionless parameters have not been varied independently of each other in the experiments the extent of which can be demonstrated by a principal component analysis of the data [9]. The approximate relations

$$<\rho_* > \sim <\beta>^{1/2} \quad , \quad <\nu_* > \sim <\beta>^{-3/2 \text{ to } 2}. \tag{12}$$

can be established from graphical representations of the data. The first relation in (12) is depicted very well in Fig. 1 which shows the ITER L-mode data [23]; the dotted line is the result of a linear regression fit. We notice that at a given value of $<\beta>$, the range of variation in $<\rho_*>$ is only by a factor ~2. Collinearities are also present in local data as a direct consequence of Eq. (12) but additionally because the profile shape functions g_n (x), g_T (x) etc. do not vary much. From an extensive range of transport interpretation calculations with the TRANSP code [24] we have selected local confinement data from six JET L-mode pulses: three steady state pulses (ρ_* scan) and non-steady state pulses (two current ramps, pellet injection and off-axis ICRH). For each data variable p_j we evaluate at each radius x the temporally averaged value and the standard deviation via

$$\left\{p_j(x,t)\right\} = \overline{p}_j(x) + \sigma_p(x) = \overline{p}_j(x)\left(1+\delta p_j(x)\right) \tag{13}$$

The angular brackets indicate an ensemble of typically 50-100 time points and δp_j is a normalised standard deviation. We examine only the range $0.3 < x < 0.8$; for $x < 0.3$ sawteeth effects cause large variations and $x > 0.8$ is excluded because of limited diagnostic capabilities.

Figures 2a-2d show the time averages of ρ_*, ν_*, β, q_ψ plotted against each other; the straight lines from linear regression fits are indicative of the inner relations (12). The relative variations around the mean are ~ of 1-10% for steady states and >10% for non-steady states. We therefore find to a good approximation that the profiles of the dimensionless parameters of F can be represented in steady state pulses by

$$\rho_*(x,t) = <\rho_*(t)> \; g_\rho(x) \; (1 + \delta\rho(x)) \tag{14}$$

The profile shape functions g_ρ etc. for steady states exhibit little pulse to pulse variations such that Eq. (14) directly reflects the collinearity problem (12). Thus in order to locally avoid data collinearities, non-steady state data with n, T, B evolving is needed.

5. TESTING MODELS AGAINST GLOBAL DATA

A prerequisite for a transport model, whether theoretical, heuristic or empirical, is that it reproduces the measured global τ_E values. An acceptable test of a model is usually based on an RMSE test

$$\left[\frac{1}{N}\sum_{n=1}^{N}(\tau_E - \tau_{model})^2 / \tau_E^2\right]^{1/2} \leq \delta_\tau \qquad (15)$$

associated with a standard regression fit to N data values. In such fits [7-9] the normalised st.d. δ_τ is of order 0.1-0.15.

We wish to estimate a level δF_{model} of the relative uncertainties (defined below) on models for F that satisfy the test (15). We assume that the models can be represented by the formula in Eq. (9) and proceed, as in section 3, to extract τ_E from the global averages which enter Eqs. like (14). Next we expand as follows

$$F_{model} = \left(1 + \Delta\tilde{F}\right) \tau_E^{x_\tau+2} \tilde{F} \left(1 + \delta F_{model}\right) \qquad (16)$$

In this expansion $\tilde{F}$ denotes the part of F without τ_E; $\Delta\tilde{F}$ denotes the relative error on calculating $\tilde{F}$ from experimental data with its associated error bars; δF_{model} represents the discrepancy between the model and the true (and unknown) F; the source of such a discrepancy could be the approximations made in a theory using correct physics or it could originate from the use of an incorrect physics model.

We insert (16) in (8) and assume that the relative error on G can be based on the Gaussian estimate

$$\Delta G^2 = \Delta g^2 + \Delta\tilde{F}^2$$

The relative error on g is also assumed to be derived from the Gaussian estimate

$$\Delta g^2 = \Delta g_n^2 + \Delta g_T^2 + \Delta g_P^2 + \Delta g_B^2$$

the experimental profile errors are defined as e.g.

$$g_T^{measured} = g_T(x,\ t)\ (1 \pm \Delta g_T\ (x)) \qquad (17)$$

where Δg_T should be sampled from a Gaussian distribution of halfwidth Δg_T (and similarly for n, B, P). After solving Eq. (8) for τ_E we get

$$\delta F_{model} = \pm (2 + x_\tau)\, \delta_\tau \pm \Delta G \tag{18}$$

Experimental errors on the profiles for n, T, P and B and those associated with the determination of $\tilde{F}$, i.e. ΔG, combine with "the confinement degradation" index $2 + x_\tau$ and δ_τ to permit a level of uncertainty, δF_{model} which substantially exceeds δ_τ in the test (15). Two simple examples may serve as an illustration; for $F_{model} = F_o$ we have $x_T = 0$, $\Delta\tilde{F} \equiv 0$; for $F_{model} = \rho_*$ we get $x_T = \frac{1}{2}$, $\Delta\tilde{F}^2 = \frac{1}{2}\,\Delta g_n^2 + \Delta g_B^2$. (For complex models with many parameters $\Delta\tilde{F}$ will of course increase). As a rough guide to Eq. (18) we find, for $\delta_\tau = 0.15$ and the Δ's of (17) assumed uniform in space and equal to say 10%,

$$0.4 \leq \delta F_{model} \leq 0.8$$

6. TESTS OF MODELS AGAINST LOCAL DATA

The test of a transport model in simulations or prediction calculations is that it reproduces the measured temperature profile to within experimental errors, i.e.

$$T_{model}/T_{data} = 1 \pm \Delta_T \tag{19}$$

where Δ_T is equal to, or of order Δ_{gT} of Eq. (17). The calculation of T_{model} is the result of integrating Eq. (2). We assume that models can include temperature and ∇T dependencies such that

$$F_{model} = \tilde{F}\; T^{x_T}\; \varepsilon_T^{x_\varepsilon} \tag{20}$$

in which the exponent x_T denotes the non-linearity while the tilde symbol means that $\tilde{F}$ does not contain T. Integration of Eq. (2) starting at x = 1 yields

$$T_{model}\ (x) = \left[T_1^{y_1} + \int_1^x \left(y_1 \frac{q\ B}{en\ |\nabla x|\ \tilde{F}_{model}} \right)^{y_2} dx \right]^{1/y_1} \tag{21}$$

where $y_1 = (2 + x_T)\, y_2$ and $y_2 = 1/(1-x_\varepsilon)$. We can again estimate the level δF_{model} of uncertainties on models for F which satisfy the test (19). The error on the integrand of (21) is now

$$\Delta h^2 = \Delta \tilde{F}^2 + \Delta g_n^2 + \Delta g_B^2 + \Delta g_P^2 \tag{22}$$

Eq. (20) is then expanded like Eq. (16) and inserted in Eq. (21). This gives

$$\delta F_{model} = \pm (x_T + 2)\Delta_T \pm \Delta h \tag{23}$$

The result is similar to that obtained for the global test in the previous section (Eq. 18). $\Delta h^2$is smaller than ΔH^2 by Δg_T^2, Δ_T is likely to be of order δ_τ and x_T will be equal to x_τ such that $x_T + 2$ can again be thought of as a degradation index. This index encapsulates the temperature "resiliency" concept studied in detail by Callen et al., [21], it permits in conjunction with experimental errors the level of discrepancy (Eq. 23) in tests like (19). In order to see how it works out in practice we examine temperature profiles from predictive model calculations with the JETTO code [25]. In these JETTO calculations Eq. (20) is evaluated as described above and in addition Maxwell's equation for B(x) is solved by a neoclassical resistivity model. Calculations have been performed for the six JET pulses described in section 3. These pulses exhibit a small parameter range of variation as regards a, n, I_ϕ, P, ε, H etc. Regression fits (like the ones made to the ITER L-mode data) of this JET local confinement data against models for F such as given by Eq. (9), do not make sense for the reasons evident from Fig. 2. At most we can test data trends and for this purpose three heuristic models have been chosen. These are represented by

$$F_1 = 3.3\ 10^{-4}\ q_\psi^2 \left(\varepsilon_T^{-1} + \varepsilon_n^{-1}\right)\frac{B}{B_\varphi}\varepsilon \tag{24a}$$

$$F_2 = 1.36\ F_1\ s^{-1} \tag{24b}$$

$$F_3 = C_3\ \rho_*\ q_\psi \left(\varepsilon_T^{-1} + 2\varepsilon_n^{-1}\right) s^{-1}\ f(p_j) \tag{24c}$$

Models 1 and 2 have been derived heuristically from detailed studies [26] of JET local transport data [17, 18, 30]. Model 3 has been developed by Rebut, Lallia and

Watkins [10] and $f(p_j)$ contains additional parameters as well as a critical gradient term. The essential difference between the models for the present purpose is that F_1, F_2 are Bohm like $\left(F \sim \rho_*^0\right)$ while $F_3 \sim \rho_*$ is gyroBohm like.

In the JET experiments on transport scaling with ρ_* [17] all parameters, ν_*, β, q_ψ, s, ε_n, ε_T are held approximately constant. The scaling with minor radius a and field B is

$$\rho_* \sim a^{-5/6}\ B^{2/3},\ T \sim a^{1/3}\ B^{2/3},\ n \sim a^{-1/3}\ B^{4/3},\ q \sim a^{-2/3}\ B^{5/3}\ F \qquad (24)$$

In these experiments it is found that $F \sim \rho_*^0$ (Bohm) is needed in q for ν_* and β to remain constant. We can therefore insert (24) in (21) to calculate what a Bohm and a gyroBohm model for F predicts, if the flux q is made to scale as Bohm. For $x_T = 0$ (Bohm) and $x_T = {}^1/_2$ (gyroBohm), Eq (21) predicts

$$T_{Bohm} \sim a^{1/3}\ B^{2/3},\ T_{gyroBohm} \sim a^{2/3}\ B^{14/15} \qquad (25)$$

Thus for a range in B of a factor 2 (2MA, 1.7 T and 4MA, 3.4T) the two predictions differ only by a factor $\sim B^{4/15}\ a^{1/3} = 1.203$. Figs. 3 a and 3b show the predicted temperature profiles at a given time for the above mentioned 2MA and 4MA pulses. All three models apparently provide a reasonable match to the data values (solid curves in Figs. 3a, 3b); the sawteeth region inside R = 3.5m is evident in Fig. 3a. The ratio (19) is plotted in Figs. 3c and 3d; for the gyroBohm model F_3 this ratio is, across the radius, systematically in excess of 10-15%. We thus see that a test like (19) of Bohm and gyroBohm models can within the experimental error levels, almost accommodate both models, although the power requirements in the experiments follow the Bohm scaling predictions.

7. EXTRAPOLATIONS

We have seen in the two previous sections how insensitive the global and local tests are to the precise details of transport models. An implication of this lack of sensitivity is that extrapolations based on various transport models, each of which can describe the data, will produce different answers. We can demonstrate this point by using the ITER L-mode database [23] which contains ~1800 data sets from twelve different Tokamaks. An extrapolation from present data towards a reactor such as ITER involves mainly a change in $<\rho_*>$ as emphasised in [15, 17].

As one model we choose the ITER89P empirical scaling law for τ_E which can be expressed as [8, 9].

$$\tau_1 = C_1 \tau_B^{0.94} <\rho_*>^{-0.08} <\nu_*>^{-0.26} <\beta>^{-0.54} \varepsilon^{-2.06} \kappa^{0.14} A^{0.64} q_\psi^{0.4} \qquad (26)$$

The ITER89P expression (25) is almost dimensionally correct and it is a Bohm type scaling. A gyroBohm form can be obtained by a fit to the L-mode data by enforcing the exponent for $<\rho_*>$ to be -1. The result is

$$\tau_2 = C_2 \tau_B <\rho_*>^{-1} <\nu_*>^{-0.275} <\beta>^{-0.05} \varepsilon^{-2.07} \kappa^{0.35} A^{1.1} q_\psi^{0.4} \qquad (27)$$

Notice that the collinearity in the L-mode data (Fig. 1 and Eq. 12) when going from (25) to (26), causes $<\rho_*>^{-1}$ to be exchanged for $<\beta>^{-1/2}$.

From the predictions offered by Eqs. (26, 27) we can calculate the fusion product $<n> <T> \tau_E \sim P\tau_E^2$ for the ITER L-mode data. Figs. 4a and 4b show the calculated values for the fusion product plotted against $<\rho_*>$. Instead of showing 1800 points we form the average for each Tokamak (see Eq. 13) but for both scaling expressions we carry out a linear regression fit to the 1800 fusion product values w.r.t. $<\rho_*>$. The linear regression fits are indicated by the two dotted lines whereas the fit to actual data is marked by a solid line We notice that each of the two dotted lines in Figs. 4a and 4b, which characterize the Bohm form (Eq. 26) and the gyroBohm form (Eq. 27), describe the data points well. The ITER89P line in Fig. 4a is however very close to the actual data (on which it is based) and so too are the two extrapolations to the ITER CDA design parameter [27] and those of a more recently proposed set [28]. The dotted line in Fig. 4b representing the gyroBohm expression offers on the other hand an optimistic extrapolation: it pushes the ITER predictions beyond the ignition margin marked by a horizontal dashed line. These discrepancies in extrapolations arise because we force the existing L-mode data to fit two different models (Eqs, 25 and 26); both fits are reasonable because of the data collinearity, but extrapolations in $<\rho_*>$ at fixed $<\beta>$ (or vice versa) will differ substantially.

8. SUMMARY

It has been demonstrated in section 4 and elsewhere that global confinement data from a variety of Tokamaks exhibits inner relations or collinearities. The same has been demonstrated for local confinement data from a limited number of JET

discharges. Such collinearities make it difficult to determine with confidence the dependence of τ_E or F upon the dimensionless parameters like ρ_*, ν_*, β, q_ψ etc. In sections 5 and 6 we have shown that the difficulties arise from three features which, when combined, permit transport models with different physics to provide for adequate descriptions of the data: i) data collinearities, ii) measurement errors and iii) confinement degradation with power. The combination of these three features give great freedom in the testing of transport models: the ITER L-mode data and JET profile data have been used in regression fits and model calculations to demonstrate why a variety of transport models can be claimed to fit the data.

To avoid data collinearities we should assemble data from *different* experiments with: A) only one parameter p_j being varied at a time or B) one parameter p_j which is collinear with another p_κ being decorrelated by using non-steady state data. Examples of type A experiments are the non-dimensional scaling experiments: the ρ_* scans on DIIID [15], TFTR [16] and JET [17]; the ν_*, β scans on TFTR [16]. Examples of type B experiments are the current ramp experiments on TFTR [29], JET [30], DIIID [31] and the off-axis heating experiments with pellet injection on JET [18].

Measurement errors have in the analysis of this paper been treated as being random in the sense that we have assumed they are sampled from a Gaussian distribution. Systematic errors, e.g. $\Delta_T = \Delta_T(B)$ for an ECE diagnostic can lead to the wrong inferences about dependencies $F = F(p_j)$. Effects from systematic errors of a given diagnostic can be partly eliminated by comparing experiments on two or more Tokamaks of different sizes. Preliminary experiments of this type have recently been carried out on JET and DIIID [32].

The degradation of confinement with power (or temperature) has been demonstrated to increase the level of uncertainty δF_{model} permitted in tests of a transport model against global τ_E data (Eq. 15) and local T_e data (Eq. 21). δF_{model} also increases with the number of independent variables in the F function. Thus to minimise the uncertainties in extrapolations towards a reactor all parameters, i.e. ν_*, β, q_ψ etc. should be kept fixed and only ρ_* should be varied. The extrapolations therefore requires a well conditioned multi-machine database from which the variation $F(\rho_*)$ can be determined. To advance the understanding of transport in a Tokamak requires additional data to establish the trends of F, w.r.t. ν_*, β and q_ψ.

Appendix A: Dimensionless Local Parameters

In the following definitions of parameters which can enter the function F of Eq. (3) B denotes the poloidal field, B_ϕ the toroidal field and x is a normalised flux surface label. A standard plasma physics notation is used and all dimensional variables are in SI units.

Geometry:

Aspect ratio $\varepsilon = ax/R_0$; Ellipticity E; triangularity Δ; (A1)

Profiles:

Scale length of n, T $\varepsilon_n^{-1} = R\nabla n / n$, $\varepsilon_T^{-1} = R\nabla T / T$;

Safety factor $q_y = \frac{RB_f}{2p} \oint \frac{dL}{R^2 B} \approx e\, E^{1/2}\, B_f / B$; shear $s = x\, q'/ q$; (A2)

Power deposition $g_p = P(x)/P = \frac{1}{P}\int_0^x q(x) \frac{1}{a} V'\, dx$;

Ratios for species:

Z_{eff}; T_e/T_i; m_p/m_e; $A = m_i/m_p$; (A3)

Plasma variables:

Larmor radius $\rho_* = \left(\frac{Am_p}{e}\right)^{1/2} \frac{T_e^{1/2}}{aB}$;

Collisionality $\nu_* = \left(\frac{e^2 \log\Lambda}{3(2\pi)^{3/2}\varepsilon_o^{\,2}}\right) \frac{naZ_{eff}}{T_e^{\,2}}$

Plasma beta $\beta = (4e\mu_o) \frac{n_e T_e + n_i T_i}{2B^2}$ (A4)

Appendix B: Dimensionless Global Parameters

We write out the expressions for the global averages of the dimensionless parameters used in e.g. [9]. A set of definitions consistent with that in Appendix A is obtained if we start from the work of Callen et al. [21] in which the appropriately density-space weighted average diffusivity is

$$<\chi>=\left[4\int_0^1 \frac{N(x)\ \ dx}{a^2\, E\, |\nabla x|^2\, n(x)\, V'\, \chi(x)}\right]^{-1} \tag{B1}$$

For $\chi = \chi_B$ and for $|\nabla x|^2 = 2\,E^2/(E^2+1)$ we get

$$<\chi_B>=\frac{1}{3e\mu_o\pi}\ \frac{\varepsilon P\tau_E}{a^2<n>I_o\,\kappa}\left(2\int_0^1 \frac{2E}{E^2+1}\ \frac{g_N\, g_B}{g_n\, g_T}\,x dx\right)^{-1} \tag{B2}$$

The edge ellipticity $E(x=1) = \kappa$ to conform with the notation used in global scaling laws. The average temperature is

$$<T> = \frac{P\tau_E}{3e<n>V} = \frac{1}{\kappa<n>}\int_0^1 \left(n_e\, T_e + n_i T_i\right) x dx \tag{B3}$$

The Bohm time used in Eq. (8) is $\tau_B = \frac{3}{4}\ a^2/<\chi_B>$. The plasma variables of Eq. (A4) become

$$<\rho_*> = \frac{(Am_p)^{1/2}}{\sqrt{6}\ e\ \mu_o}\left(\frac{\varepsilon P\tau_E}{a^3<n>I_o^2\kappa}\right)^{1/2}\ ;\quad <\beta> = \frac{8}{3\mu_o}\ \frac{\varepsilon P\tau_E}{a I_o^2}$$

$$<\nu_*> = 3\sqrt{2}\,\pi^{5/2}\ \frac{e^4 \log\Lambda\, Z_{eff}}{\varepsilon_o^2}\ \frac{a^7<n>^3\kappa^2}{\varepsilon^2 P^2 \tau_E^2} \tag{B4}$$

The inverse relations of (B4) + τ_B are given in [9].

Appendix C: Transport Models

We list a number of theoretical, empirical and heuristic transport models for the diffusivity χ as represented by Eq. (3) (see also [12, 20]). If the transport model gives only an expression for τ_E like Eq. (10) the F function is derived from Eq. (10a) using the definitions in Appendix B. References are given and possible

residual dependencies of F are omitted as are numerical constants. The numbers in curly bracket represent $x_\tau + 2$ of Eq. 10a.

1.	Electrostatic Vlasov or pure Bohm [7]		$F = F_o$	{2}
2.	Short wavelength or pure gyroBohm [1-5]		$F = \rho_*$	{2.5}
3.	Ideal MHD [33]		$F = \rho_*^{-1}\, \beta^{-1/2}$	{1}
4a.	Resistive MHD,	S^o [12]	$F = \rho_*\, \nu_*\, \beta^{-1}$	{–0.5}
4b.		$S^{-1/2}$	$F = \rho_*^2\, \nu_*^{3/2}\, \beta^{-5/4}$	{–1.25}
4c.		$S^{1/2}$ [34]	$F = \nu_*^{1/2}\, \beta^{-3/4}$	{0.25}
4d.		S^1	$F = \rho_*^{-1}\, \beta^{-1/2}$	{1}
5.	η_i modes [35]		$F = \rho_*\, s^{-1}\, \varepsilon_n\, (T_e/T_i)^{-1}\, (\eta_i - 2/3)^{1/2}$	{2.5}
6.	DTIM [36]		$F = \rho_*\, \nu_*^{-1}\, s^{-2}\, \varepsilon_n^{-1}\, q_\psi^{-1}\, \varepsilon^{1/2}\, A^{-1/2}$	{4.5}
7.	Drift waves [37]		$F = \rho_*\, s^{-1}\, \varepsilon_n^2\, \varepsilon^2\, (\nu_*\, q_\psi)^{0 \text{ or } 1}$	{2.5}
8.	Resistive fluid Turbulence [12]		$F = \rho_*\, \nu_*\, \beta^{-1/2}\, A^{-1/2}$	{0}
9.	Rebut-Lallia-Watkins	[10]	$F = \rho_*\, \nu_*^{1/2}\, \beta^{-1/2}\, (1-\varepsilon)\, s^{-1}\, q_\psi\, (\varepsilon_T^{-1} + 2\, \varepsilon_n^{-1})\, (T_e/T_i)^{1/2}\, A^{1/2}\, (1+Z_{eff})^{1/2}$	{1}
10.	ITER L-thermal [9]		$F = \nu_*^{0.15}\, \beta^{1.21}$	{2.9}
11.	Goldston [7]		$F = (ax)^{0.26}\, \beta/\chi_B$	{2.0}
	The nearest dimensionally correct form is		$F = \rho_*^{0.18}\, \nu_*^{0.34}\, \beta^{0.36}$	{1.77}
12.	ITER89P [8]		$F = \rho_*^{0.08}\, \nu_*^{0.26}\, \beta^{0.54}\, \varepsilon^{2.06} \kappa^{-0.14}\, A^{-0.64}\, q_\psi^{-0.4}$	{1.82}

The Lundquist number $S = \rho_*^{-2}\ \nu_*^{-1}\ \beta^{1/2}$ is used to produce various resistive MHD scalings. The model 9 features an additional critical gradient term [10, 16]. The empirical scaling laws 11 and 12 have been transformed to dimensionally correct forms by adjusting the exponents z of Eq. (7b) by δz as follows: Goldston $\delta_n = \delta_I = \delta_P = -\delta_a = 0.052$ and ITER89P $\delta_n = \delta_I = \delta_P = -\delta_a = 0.048$.

ACKNOWLEDGEMENTS

The authors acknowledge the members of the JET team for making available the data used in this study.

REFERENCES

[1] FURTH, H.P., Nucl. Fusion 13 (1973) 495. Review.

[2] KILLEEN, J., Nucl. Fusion 16 (1976) 841. Review.

[3] DÜCHS, D.F., FURTH, H.P., RUTHERFORD, P.H., in Plasma Physics and Controlled Nuclear Fusion Research (Proc. 4th Int. Conf. Madison 1971) 1, IAEA Vienna (1971) 369.
MERCIER, C., SOUBBARAMAYER, BOUJUT, J.P., ibid p. 425
DNESTROVSKII, Y.N., KOSTOMAROV, D.P., PAVLOVA, N.L., Energy Balance in Devices of the Tokamak Type considering charge exchange, Translation in PPL Report MATT-TRANS-107, Princeton 1971.

[4] HUGILL, J., Nucl. Fusion 23 (1983) 331. Review.

[5] KAYE, S.M., GOLDSTON, R.J., BELL, M. et al.,
Nucl. Fusion 24 (1984) 1303

[6] BECKER, G., Nucl. Fusion 24 (1984) 1364.

[7] GOLDSTON, R.J., Plasma Physics Contr. Fusion 26 (1984) 27.

[8] YUSHMANOV, P.N., TAKIZUKA, T., RIEDEL, K.S., et al.,
Nucl. Fusion 30 (1990) 1999.

[9] CHRISTIANSEN, J.P., CORDEY, J.G., KARDAUN, O.J.W.F., THOMSEN, K., Nucl. Fusion 31 (1991) 2117.

[10] REBUT, P.H., WATKINS, M.L., GAMBIER, D.J., BOUCHER, D., Phys. Fluids B, 3 (1992) 2209.

[11] GHANEM, E.M., SINGER, C.E., BATEMAN, G., STOTLER, D.P., Nucl. Fusion 30 (1990) 1595.

[12] CONNOR, J.W., WILSON, H.R., Survey of theories of anomalous transport, Internal note, AEA Fusion Culham Laboratory. To be submitted to Plasma Physics and Controlled Fusion.
CONNOR, J.W., MADDISON, G.P., WILSON, H.R., et al. An assessment of theoretical models based on Observations in the JET Tokamak, Part I: Ion Heat transport due to ∇T_i instabilities, JET preprint JET-P(92)63, JET Joint Undertaking, submitted to Plasma Physics and Controlled Fusion.

[13] KADOMTSEV, B.B., Sov. J. Plasma Physics 1 (1975) 295.

[14] CONNOR, J.W., TAYLOR, J.B., Nuclear Fusion 17 (1977) 1047.

[15] WALTZ, R.E., DEBOO, J.C., ROSENBLUTH, M.W., Phys. Rev. Lett 65 (1990) 2390
WALTZ, R.E., DEBOO, J.C. OSBORNE, T.H., Nucl. Fusion 32 (1992) 1051.

[16] PERKINS, F.W., BARNES, C.W., JOHNSON, D.W., SCOTT, S.D., et al., Nondimensional Transport Scaling in the Tokamak Test Fusion Reactor: Is Tokamak Transport Bohm or GyroBohm?, to appear in Phys. Fluids.

SCOTT, S.D., BARNES, C.W., MIKKELSEN, D.R., PERKINS, F.W., in Plasma Physics Controlled Nuclear Fusion Research, 1992, 14th Int. Conf. Wurzburg, Paper IAEA-CN-56/G-3-3.

[17] CHRISTIANSEN, J.P. BALET, B., BOUCHER, D., CHALLIS, C., et al., Plasma Physics and Controlled Fusion, 34 (1992) 1881.

[18] BALET, B., CORDEY, J.G., MUIR, D.G., SCHMIDT, G.L., Nucl. Fusion 32 (1992) 1261.

[19] TAYLOR, J.B., MCNAMARA, B., Phys. Fluids 14 (1972) 1492.

[20] CONNOR, J.W., Plasma Physics Contr. Fusion 20 (1988) 619.

[21] CALLEN, J.D., CHRISTIANSEN, J.P., CORDEY, J.G., THOMAS, P.R., THOMSEN, K, Nucl. Fusion 27 (1987) 1857.

[22] CHRISTIANSEN, J.P., CORDEY, J.G., THOMSEN, K., Nucl. Fusion 30 (1990) 1183 (see Tables IV -VI).

[23] KAYE, S.M., BARNES, C.W., BELL, M.G., Phys. Fluids B 2 (1990) 2926.

[24] HAWRYLUK, R.J., An empirical approach to Tokamak Transport, Proc. Course and Workshop, Varenna, 1979, Vol. 1, p. 19, Rep. EUR-FU-BRU/XII/476/80, CEC, Brussels (1980) Goldston, R.J., J. Comp. Phys. 43 (1981) 61. SMITHE, D.N., et al., Nucl. Fusion 27 (1987) 1319.

[25] CENACCHI, KG., TARONI, A., JET10: A free boundary plasma transport code, JET Internal Report JET-IR (88) 03, 1988. JET Joint Undertaking.

[26] TARONI, A., Heuristic transport models of the Bohm type. To be published.

[27] TOMABECHI, K., GILLELAND, J.R., SOKOLOV, Yu. A., TOSCHI, R. and the ITER team, Nucl. Fusion 31 (1991) 1135.

[28] REBUT, P.H., BOUCHER, D., GAMBIER, D.J., KEEN, B.E., WATKINS, M.L., The ITER Challenge, 17th SOFT, Rome, September 1992, JET Preprint JET-P(92) 92, JET Joint Undertaking.

[29] ZARNSTORFF, M.C. et al., in Plasma Physics and Controlled Nuclear Fusion Research, 1990 (Proc. 13th Int. Conf. Washington) Vol. 1, IAEA, Vienna (1991) 119.

[30] CHALLIS, C.D., CHRISTIANSEN, J.P., CORDEY, J.G., GORMEZANO, C. et al., Nucl. Fusion 32 (1992) 2217

[31] FERRON, J.R., LAO, L.L., TAYLOR, T.S., 19th EPS Conf. on Controlled Fusion and Plasma Physics, Vol. 16C, 55, Innsbruck (1992).

[32] CARLSTROM, T. N., CHRISTIANSEN, J.P., DEBOO, J.C., WALTZ, R.E., ρ_* scaling of Confinement in dimensionally similar discharges in JET and DIIID, 34th APS Meeting Seattle (1992), 3E5, page 1410, Bulletin of the American Physical Society, Vol. 37, No. 6, November 1992.

[33] BICKERTON, R.J., Indications from Dimensional Analysis of the L-mode Database, Rep. FRCR 374, Texas Univ., Austin (1990).

[34] THOMAS, P.R., A Comparison Between Additional Heating Data and Forms with Model Scale Invariance. Preprint JET P (87) 17, JET Joint Undertaking (1987).

[35] HONG, B.G., HORTON, W., Phys. Fluids B2 (1990) 979.

[36] DIAMOND, P.H., BIGLARI, H., Phys. Rev. Lett. 65 (1990) 2865.

[37] WALTZ, R.E., DOMINGUEZ, R.R., WONG, S.K., et al., in Plasma Physics and Controlled Nuclear Fusion Research 1986 (Proc. 11th Int. Conf. Kyoto, 1986), Vol. 1, IAEA, Vienna (1987) 345.

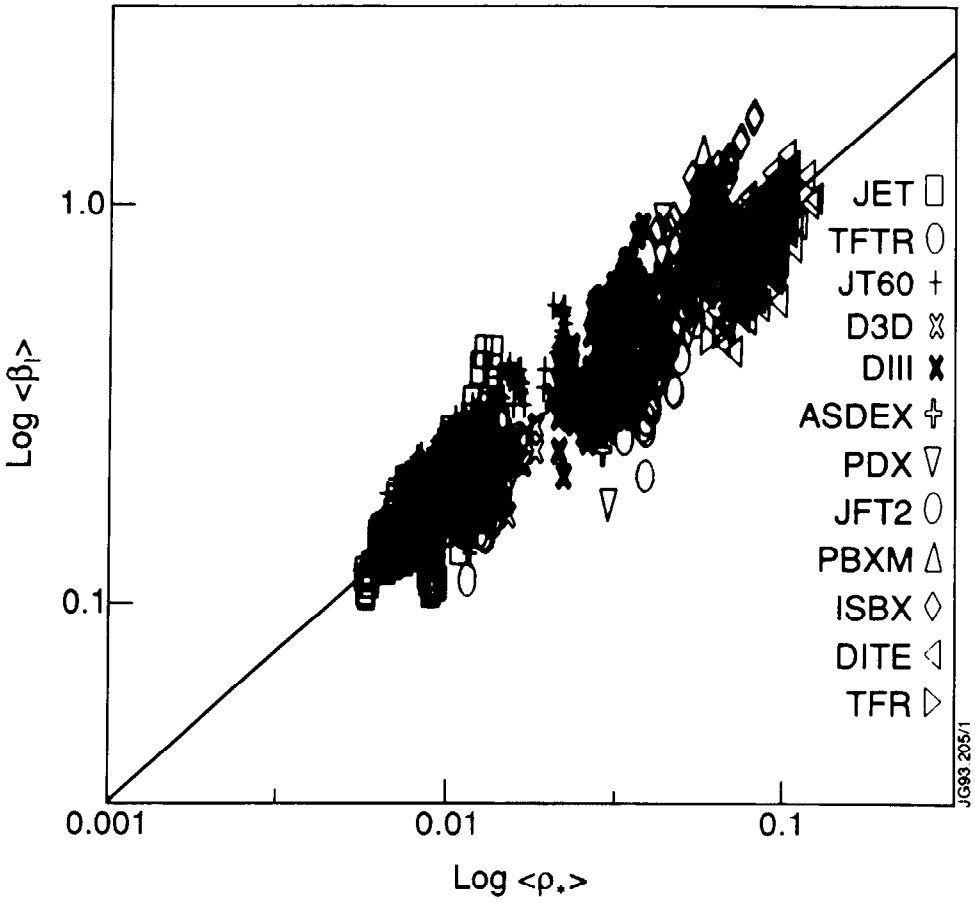

Figure 1. The ITER L-mode data on $\langle\rho_*\rangle$ vs $\langle\beta\rangle$ shows collinearities: at a fixed value of $\langle\beta\rangle$, $\langle\rho_*\rangle$ varies only by a factor 2.

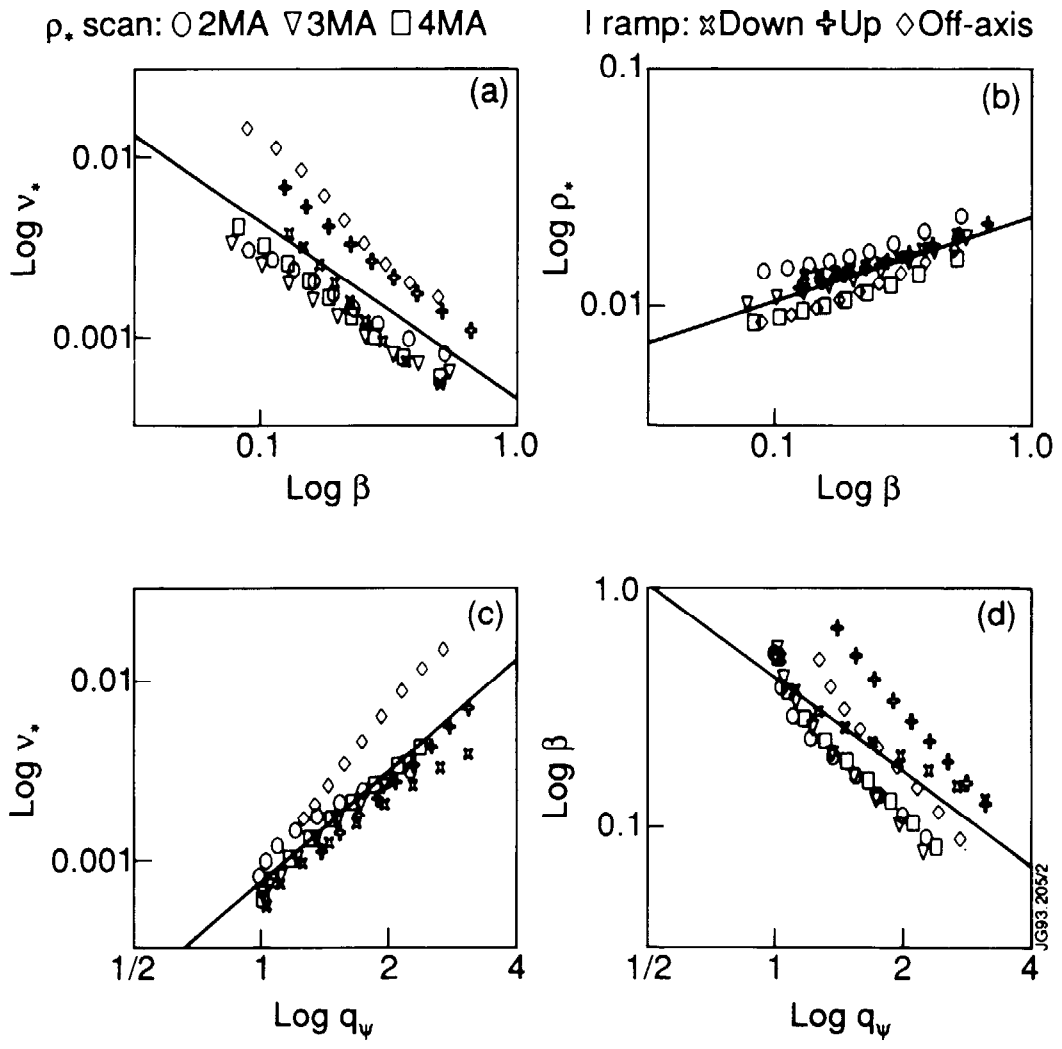

Figure 2. Averages (Eq. 13) of local dimensionless parameters show collinearities when plotted against each other. The six symbols refer to six different JET discharges.

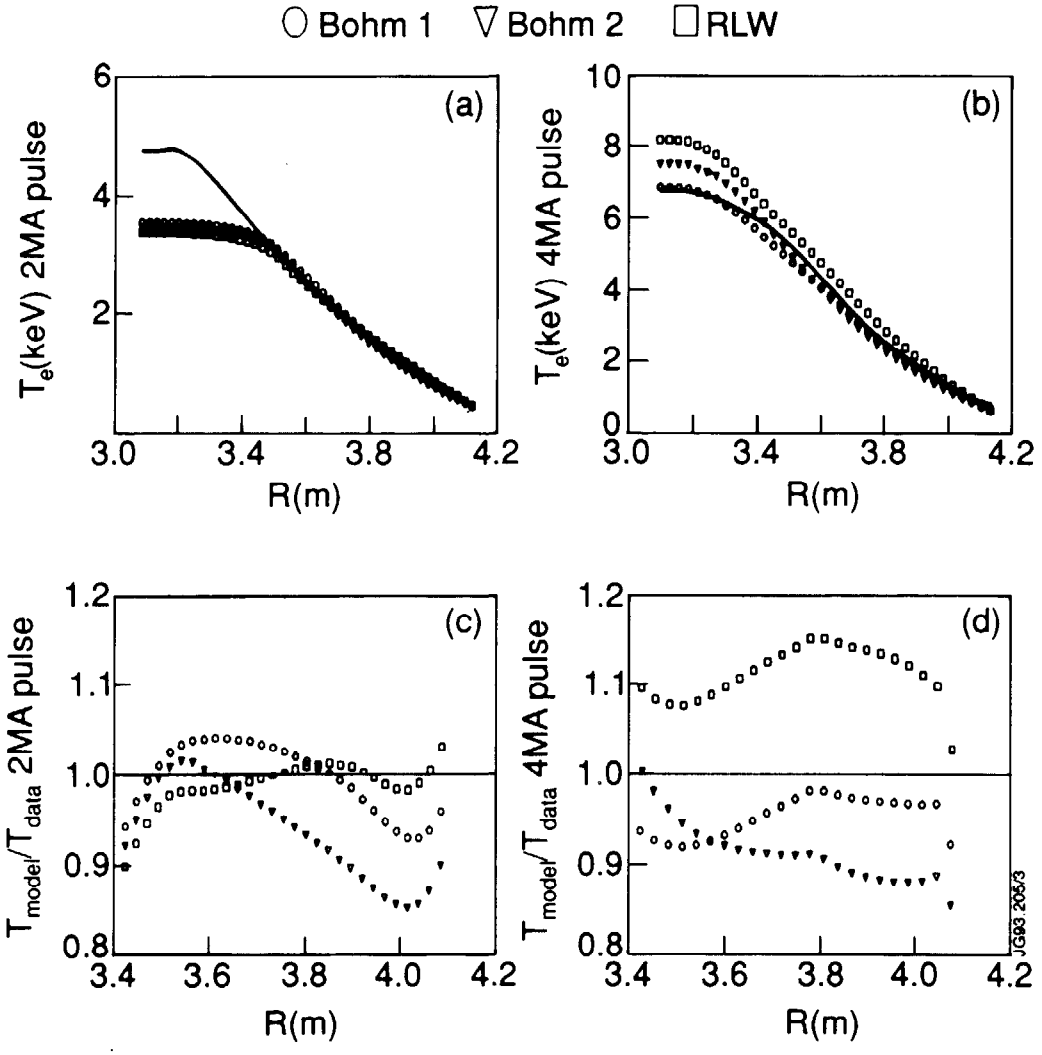

Figure 3. Predicted and measured temperature profiles $T_e(R)$ for the models given by Eq. (24); a) a 2MA JET pulse, b) a 4MA JET pulse, c) and d) show the ratio between predicted and data values. Predictions are made by the JETTO code [25].

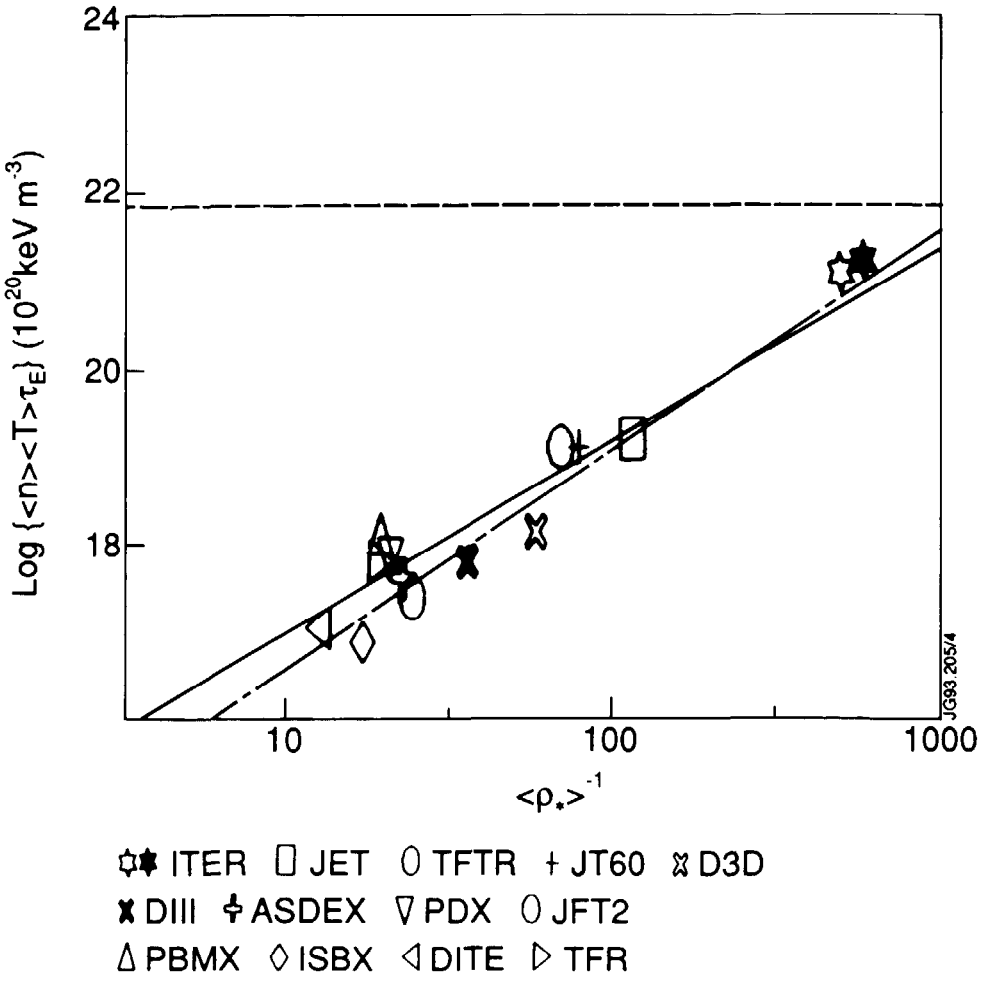

Figure 4. a) Values of <n> <T> τ_E predicted by the ITER89P scaling law [8] versus <ρ_*>. Each symbol represents the database average for a Tokamak and the two stars refer to the ITER CDA design parameters [27] (open star) and the parameters of [28] (full star). The solid line represents a linear regression fit to the 1800 ITER L-mode data values of <n> <T> τ_E vs <ρ_*>. The dotted line represents the fit to the IETR89P predicted values. The dashed line at 7 10^{20} keVm^{-3} represents the ignition level for ITER.

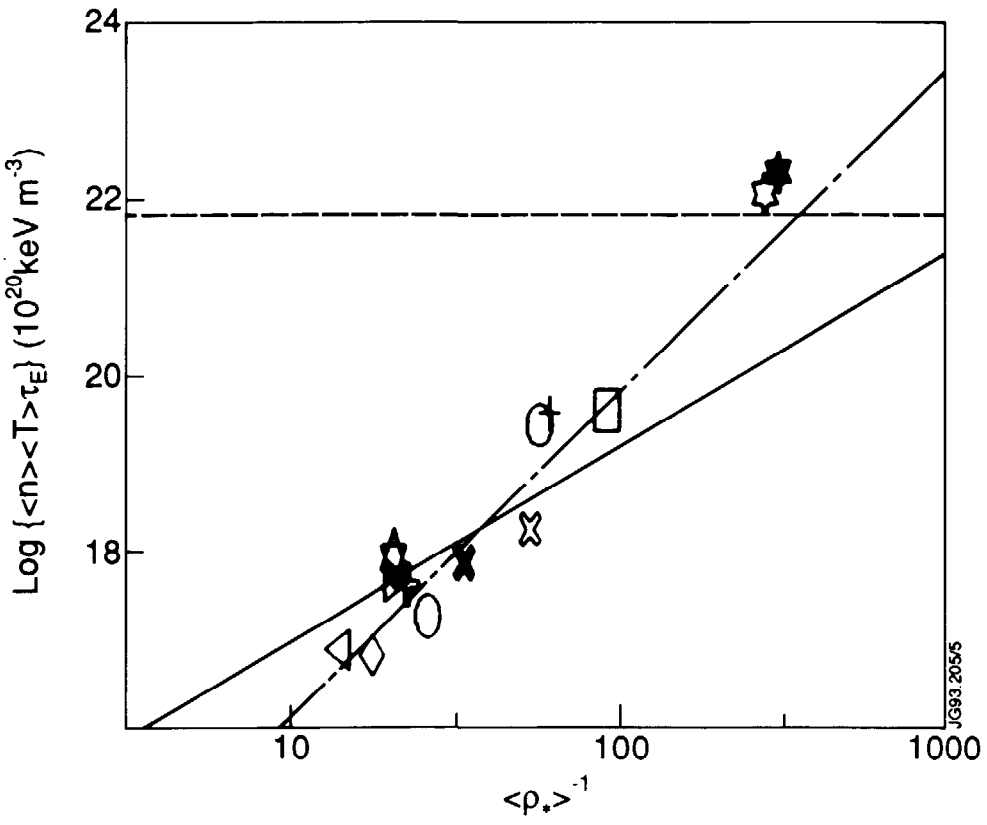

Figure 4. b) As figure 4a but the predictions are made with a gyroBohm form of ITER89P (see text). Whilst the dotted line represents the data, extrapolations towards ITER now depart significantly from the solid line.